Level-set simulations of sheared 2D foams

Y. Mezache[a], M. Le Merrer[a], F. Detcheverry[a], A.-L. Biance[a], P. Spelt[b]

a. Institut Lumière Matère, Universitè Claude Bernard Lyon 1, yedhir.mezache@univ-lyon1.fr
b. Laboratoire de Mécanique des Fluides et d'Acoustique, Ecole Centrale de Lyon

Abstract :

A liquid foam is a dispersion of gas bubbles in a soapy liquid matrix. It is a yield-stress material, solid-like at low stresses and which can flow under sufficiently large external stresses. Liquid foams are used in a diverse array of applications for their large specific area, light weight, and insulating properties. Foams have a multi-scale structure : they are composed of millimetric bubbles separated by submicrometric films whose surfaces are covered with monolayers of surfactant molecules. The stability and rheology of foams depend strongly on the type of surfactants used to generate them, and the link between micro and macro scales remains an active area of research. Here we investigate this link at the bubble scale by numerical simulations. We focus on the elementary topological rearrangements, called T1 events, in a two-dimensional arrangement of bubbles submitted to shear. We use a two-phase flow level-set method that has been adapted to include surfactant dynamics (Titta et al., Journal of Fluid Mechanics, 2018) and extend this parametric study. In particular, we examine how the adsorption depth, a measure of surfactant distribution between the bulk and surface, influences energy dissipated in the flow. Our simulations show that the integrated rate of viscous dissipation does not account for all the work expended in the material during T1 events. We explain this observation in terms of a surface dissipation generated through Marangoni stresses and surfactant adsorption/desorption mechanisms occurring at the gas-liquid interfaces. We investigate how the adsorption depth affects surfactant transport and energy dissipation in the system.

Key words : bubble dynamics, foams, interfacial flows

1 Introduction

Liquid foams consist of assemblies of gas bubbles in a soapy liquid matrix. Because of their light weight, large specific area, mechanical and insulating properties, foams are in demand for a wide variety of practical applications. In construction, for example, lightweight structural and insulating materials can be produced from precursory liquid foam mixtures (e.g. foam concrete and spray foam insulation). For fighting fires, large volumes of foam can be generated with little raw material. Other major areas of foam use include food processing, chemical processing and decontamination. Therefore, in order to tailor foams for their varied applications, it is important to understand their mechanical properties, namely their stability and rheology. These macroscopic mechanical properties are known to depend heavily on the type of surfactant molecules used to generate the foam [1]. Details of the interactions between mechanisms at microscopic and macroscopic scales so far remain unclear.

At the macroscopic scale, a foam is considered as a continuous medium described by constitutive laws. Classified as a complex yeild-stress fluid, liquid foams are solid-like at low stresses, but flowing under large external stresses [2]. However the multiplicity of length and time scales found within its structure makes modeling its rheology particularly difficult. Focusing inwards from the macroscopic scale, liquid foams are composed of milimetric gas bubbles separated by a net of sub-micrometric liquid films, which contain nanometric monolayers of surfactants at both gas-liquid interfaces (Figure 1). The surfactant monolayers act as a stabilizing agent at interfacial and film scales, inhibiting film rupture. During shear deformation at the bubble scale, surfactant transport at film and interfacial scales feedback on the two-phase flow.

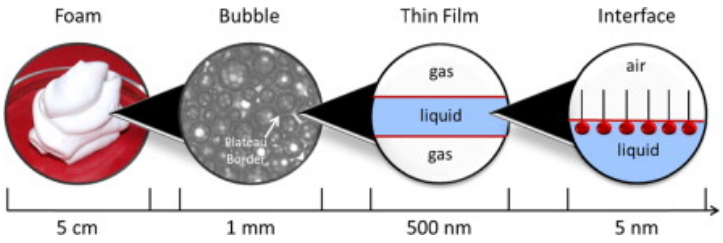

FIGURE 1 – Foams contain structures at multiple scales. The global dynamical behavior of the foam results from a complex interaction of the different physical mechanisms produced at each scale. Reproduced from [3].

When liquid foams are submitted to shear, a rearrangement occurs at the bubble scale. This is defined as a T1 process, shown in Figure 2. Bubbles 1 and 2 move to the right as bubbles 3 and 4 move to the left. During a T1 event, the film separating neighboring bubbles 2 and 3 is eventually collapsed to an unstable vertex joining all four bubbles, then a new film is spontaneously produced. The newly created film results in switched neighbors, and thus a new configuration.

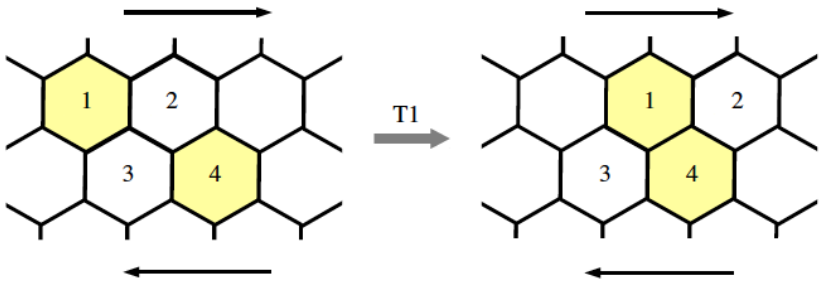

FIGURE 2 – Schematic view of a T1 rearrangement of 2D bubbles. Reproduced from [4].

In this study, we investigate a T1 rearrangement as a dynamical process influenced by the interplay of the effects of fluid flow, surface tension, surfactant transport. The coupled dynamics are complex and hard to describe because they occur and interact at multiple scales (Figure 1). We, therefore, approach this problem using numerical simulations. The level-set method is used here in large part because it gives a simple method for tracking interfaces, where the surfactant transport and flow dynamics are coupled. Here, we investigate the effects of soluble surfactants on foam flows at the bubble scale.

The physical problem and the numerical methods are presented in some detail in sections 2 and 3. Section 4 contains a description and results from an extended parametric study. More specifically, we

present an investigation on the effects of the adsorption depth on surfactant distribution and energy dissipation during T1 events. A summary and perspectives are given in section 5.

2 Physical problem : A sheared 2D liquid foam

2.1 Geometric configuration

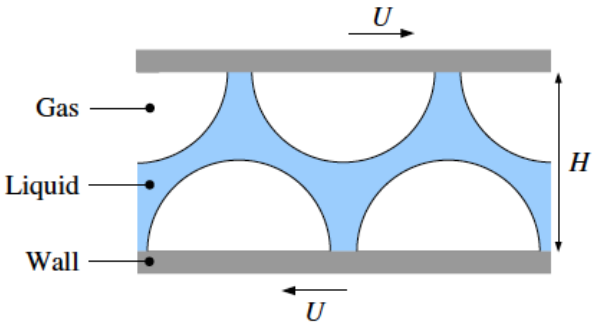

FIGURE 3 – Initial configuration : hemispherical bubbles in a liquid phase, confined between parallel moving plates. Reproduced from [4].

We consider an initial hexagonal arrangement of 2D hemispherical bubbles attached to upper and lower impermeable walls, with a distance of $\frac{2H}{\sqrt{3}}$ between nearest bubble centers (Figure 3). The shear flow is imposed by the velocity $\pm U$ at the walls. Periodic boundary conditions are imposed at the inlet and outlet of the flow, such that, for example, a bubble exiting the domain to the right reenters at the left.

2.2 Flow dynamics

Fluids in both phases are assumed to be incompressible. Thus, the Navier-Stokes equations take the form :

$$\nabla \cdot \mathbf{u} = 0, \tag{1}$$

$$\rho\big(\frac{\partial \mathbf{u}}{\partial t} + (\mathbf{u} \cdot \nabla)\mathbf{u}\big) = \nabla \cdot \sigma \tag{2}$$

where σ is the stress tensor for an incompressible, Newtonian fluid : $\sigma = -p\mathbf{I} + \mu(\nabla\mathbf{u} + (\nabla\mathbf{u})^T)$. Equations 1 and 2 govern the flow in each phase, i, with respective densities and viscosities, ρ_i and μ_i. At the walls, we assume a no-slip condition.

At the interfaces between the two phases, there is a dynamic boundary condition imposed by the stresses at the interfaces :

$$[\sigma \cdot \mathbf{n}] = -\gamma C\mathbf{n} - \nabla_s\gamma. \tag{3}$$

Here, the brackets denote $[x] = (x_{liq} - x_{gas})$, and $\mathbf{n}$ is the unit normal vector at interfaces, which points outwards from the gas to the liquid (Figure 4). γ is the local surface tension, $C = -\nabla \cdot \mathbf{n}$ is the local interface curvature, and $\nabla_s = I_s \cdot \nabla$ is the gradient along the interface. The left hand side of equation 3 represents the total jump in traction across the interface. The normal component of this jump, $-\gamma C\mathbf{n}$, is the contribution from the Young-Laplace equation, which gives the force balance between the pressure jump at the interface and the surface tension. The tangential component of the jump in traction, $\nabla_s\gamma$,

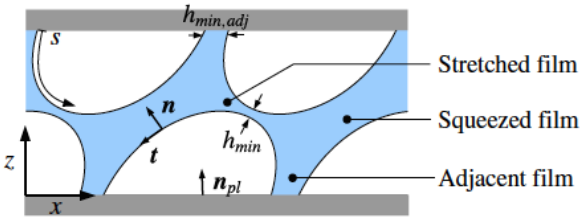

FIGURE 4 – Shearing flow regime. Reproduced from [4].

are the Marangoni forces due to variations in surface tension along the interfaces. We will see in the next section how surface tension varies in the interface with changes in local surfactant concentration.

2.3 Surfactant transport and surface tension

The surfactant concentrations in the liquid phase and at the interface are initially uniformly distributed, and are transported by the flow when the plates are set into motion.

Both within the liquid phase and at the interface, surfactants are transported by advection and diffusion mechanisms. In the liquid phase, transport of surfactant concentration, F, is described by :

$$\frac{\partial F}{\partial t} + \nabla \cdot (F\mathbf{u}) = D_F \nabla^2 F, \tag{4}$$

where F is the amount of surfactants per unit volume, and D_F is the coefficient of diffusion in the liquid. Transport of surfactant concentration along the interface, f, is :

$$\frac{\partial f}{\partial t} + \nabla_s \cdot (\mathbf{u}f) = D_f \nabla_s^2 f + j \tag{5}$$

where f is the amount of surfactants per unit area, D_f is the coefficient of diffusion at the interface, and ∇_s is the gradient along the interface. Equation 5 involves a source term j, arising from the fact that surfactant is simultaneously exchanged between the interface and nearby fluid : $j = -D_F \nabla F \cdot \mathbf{n}$. The attachment and detachment of surfactant molecules to and from the interface are called adsorption and desorption, respectively. The source term is [5] :

$$j(f, F) = r_a F_s (f_\infty - f) - r_d f \tag{6}$$

Here r_a and r_d are adsorption and desorption rate coefficients, f_∞ is the saturated interface concentration, and F_s is the concentration in the liquid phase near the interface.

There is no surfactant flux across the upper and lower plates. So, the boundary condition for liquid bulk concentration transport at the walls is :

$$\mathbf{n}_{\text{pl}} \cdot \nabla F = 0, \tag{7}$$

where $\mathbf{n}_{\text{pl}}$ is the unit normal vector to the wall pointing into the fluid (Figure 4). For interface concentration transport at the walls, the no-flux boundary condition is :

$$\mathbf{t} \cdot \nabla f = 0, \tag{8}$$

where $\mathbf{t}$ is the unit tangent vector to the interface at the wall.

Finally, a closure relation is required for the local surface tension at interfaces, which varies with local surfactant concentration. This is derived from the Langmuir adsorption model, and appears as [5] :

$$\gamma(f) = \gamma_0 \left[1 + \frac{RTf_\infty}{\gamma_0} \ln\left(1 - \frac{f}{f_\infty}\right) \right], \tag{9}$$

where R, T, and γ_0 are respectively the ideal gas constant, temperature (constant), and surface tension for interfaces with no surfactant ($f = 0$).

During T1 events, the system behavior is the result of the coupled problems of fluid flow, interface evolution and surfactant transport. The fluid motion is governed by the Navier-Stokes equations (1,2) and the boundary conditions at liquid-gas interfaces (3). These boundary conditions involve the surfactant concentration (9), which is in turn advected and diffused by the velocity field (4, 5). This feedback between the flow and surfactant transport is a complex problem. In this study, we investigate the choreography of these dynamics and the resultant rheological behavior by numerical simulation.

3 Numerical Method - Level Set

3.1 Level-set function

The governing equations given in the previous section are defined separately for each phase occupying the physical domain. The solutions to these governing equations must also satisfy boundary conditions at the interfaces, in particular, equation 3. The idea of interface-capturing numerical methods is to formulate an expression of each governing equation that is valid over the entire domain. These typically introduce a scalar field, defined in the entire system, from which the interface location can readily be obtained. Of the various interface-capturing methods, we shall use the so-called level-set method. Define a level-set function :

$$\phi(\mathbf{x}, t) = \begin{cases} d \text{ for } \mathbf{x} \text{ in the liquid phase (film)}, \\ 0 \text{ for } \mathbf{x} \text{ at interface (film)}, \\ -d \text{ for } \mathbf{x} \text{ in gas phase (bubble)}. \end{cases} \tag{10}$$

Here, d is the distance between the material point, $\mathbf{x}$, and the nearest interface. At each time step the level set function is advected :

$$\frac{\partial \phi}{\partial t} + \mathbf{u} \cdot \nabla \phi = 0, \tag{11}$$

and interfaces are recaptured as the zero level set, $\phi(\mathbf{x}, t) = 0$. This allows interfaces to be tracked on a fixed Cartesian grid. At each time step, a re-initialization procedure is used to ensure the level-set function remains a signed distance function. The unit normal vector, to the interface can be expressed in terms of the level-set function :

$$\mathbf{n} = \frac{\nabla \phi}{|\nabla \phi|} \tag{12}$$

where derivatives are taken at $\phi = 0$. The interface curvature, $C = \nabla \cdot \mathbf{n}$, can thus be obtained with equation 12.

If we replace the two Navier-Stokes equations for each phase with a single one for the entire domain, the density and viscosity expressions become position dependent. The level set function is used to determine their local value :

$$\rho(\phi) = \rho_{liq} H_\epsilon(\phi) + \rho_{gas}(1 - H_\epsilon(\phi)), \tag{13}$$

$$\mu(\phi) = \mu_{liq} H_\epsilon(\phi) + \mu_{gas}(1 - H_\epsilon(\phi)), \tag{14}$$

where $H_\epsilon(\phi)$ is a smoothed Heaviside function, with a smoothing parameter, ϵ :

$$H_\epsilon = \begin{cases} 0 & \text{if } \phi < -\epsilon, \\ \frac{1}{2}\left(1 + \frac{\phi}{\epsilon} + \frac{1}{\pi}\sin\left(\frac{\pi\phi}{\epsilon}\right)\right) & \text{if } |\phi| \leq \epsilon, \\ 1 & \text{if } \phi > \epsilon. \end{cases} \tag{15}$$

3.2 Distribution form of governing equations

Now, the governing equations can be written in distribution form, in which the physical parameters at every point in the domain are expressed in terms of $H_\epsilon(\phi)$ as in equations 13 and 14. The boundary conditions at the interfaces Γ become source terms in the governing equations, via the Dirac delta function, $\delta_\Gamma = |\nabla(H_\epsilon)|$. The distribution form of the Navier-Stokes equation is [5] :

$$\rho\left(\frac{\partial \mathbf{u}}{\partial t} + (\mathbf{u} \cdot \nabla)\mathbf{u}\right) = -\nabla p + \nabla \cdot \left(\mu(\nabla \mathbf{u} + (\nabla \mathbf{u})^T)\right) + \gamma C \mathbf{n} \delta_\Gamma + \nabla_s(\gamma)\delta_\Gamma, \tag{16}$$

and the continuity equation remains $\nabla \cdot \mathbf{u} = 0$. The Laplace and Marangoni stresses at the interfaces appear in the last two terms on the right hand side of equation 16

Similarly, the distribution form of the surfactant transport equations 4 and 5 are [5] :

$$\frac{\partial}{\partial t}(H_\epsilon F) + \nabla \cdot (H_\epsilon F \mathbf{u}) = D_F \nabla \cdot (H_\epsilon \nabla F) - \delta_\Gamma j, \tag{17}$$

$$\frac{\partial}{\partial t}(f \delta_\Gamma) + \nabla \cdot (f \delta_\Gamma \mathbf{u}) = D_f \nabla \cdot (\delta_\Gamma \nabla f) + \delta_\Gamma j. \tag{18}$$

F and f are continuous functions of position throughout the domain, with source term, $\delta_\Gamma j$, corresponding to the boundary condition at interfaces. At the walls, the boundary conditions listed previously remain unchanged (eq.s 7, 8). This system is simulated numerically using a two-phase flow level-set solver extended by Titta et al. to include surfactant dynamics [6].

3.3 Parametric study

A set of dimensionless parameters characterizing different aspects of the dynamical system can be extracted from the non-dimensionalized governing equations [4]. Here, we briefly discuss parameters that are pertinent to our current investigations of the coupled dynamics of fluid flow, interface evolution, and surfactant transport :

— $\boxed{Re \equiv \frac{\rho_l H U}{\mu_l}}$ **Reynolds number** is a measure of the relative influence of inertial and viscous forces in the flow. H and U are characteristic values of length and shear velocity of the flow, respectively. $Re = 1$.

— $\boxed{Ca_{eq} \equiv \frac{\mu_l U}{\gamma_e}}$ **Capillary number** is the ratio of viscous forces to surface tension. It is defined for some equilibrium interfacial concentration, f_e, through the Langmuir equation of state (eq. 9). The capillary number is fixed at some small value ($Ca_{eq} = 0.1$).

— $\boxed{Pe \equiv \frac{UH}{D}}$ **Péclet number** is a ratio of the strengths of advective and diffusive mechanisms of surfactant transport. This parameter intervenes in the surfactant transport equations, and influences homogeneity of surfactant distribution. It depends on the local diffusion coefficient, D, and so is defined separately in the liquid bulk and at the interface (Pe_F and Pe_f).

— $\boxed{Bi \equiv \frac{r_a H}{U}}$ **Biot number** is a ratio of desorption and advection timescales. $r_d = r_a$ for this study. So, the Biot number is an index of the relative rates of deformation and surfactant exchange in the interfaces.

— $\boxed{h \equiv \frac{f_e}{HF_e}}$ **Adsorption depth** is a ratio of the surfactant concentration at the interface and in the bulk. This value is a factor of the source term in the dimensionless concentration transport equation for the liquid phase. It may be a measure of availability for exchange of surfactant in the neighborhood of interfaces.

The influences of capillary number, Péclet number, and Biot number on this system have been extensively studied, fixing $h = 1$ [4]. Results of investigations of the effects of the adsorption depth are presented in the following section.

4 Results

The adsorption depth, defined as : $h = \frac{f_e}{HF_e}$, appears as a factor in the source term for the bulk transport equation, (4), in dimensionless form. It is a measure of the relative amount of surfactant at the interfaces and in the liquid bulk at thermodynamic equilibrium. In the limit of large adsorption depth ($h >> 1$), surfactants are effectively insoluble. Here, rather, we investigate effects of reduced adsorption depths ($1 > h > 0.01$) in different Péclet regimes ($Pe = 1,\ 100$); first on surfactant distribution in the fluid, and subsequently on the mechanical response to steady wall-imposed shear. For all results presented below, we consider equal bulk and surface Péclet numbers ($Pe_F = Pe_f$), and the remaining dimensionless numbers are fixed at : $Re = 1$, $Ca = 0.1$, $Bi = 10$.

4.1 Surfactant distribution

We present here the influence of adsorption depth on the distribution of surfactant concentration during a steady, wall-imposed shear. We first consider $Pe = 100$, where diffusion of surfactants is weak both in the bulk and at the surface. Before the flow starts, surfactant concentration is homogeneously distributed, both in the liquid and its surface, and at thermodynamic equilibrium ($F_e = f_e = 1$). After the walls are set into motion, bubbles become stretched in film regions where interfaces slip past each other, and are compressed near Plateau borders where opposite interfaces move either towards or away from each other. Figure 5 shows the liquid bulk concnetration of surfactants of bubble assemblies during such T1 rearrangements. Simultaneous snapshots are shown for two simulations with $h = 1$ and $h = 0.01$ in figures 5(a) and 5(b), respectively. In both cases, the liquid is depleted by adsorption onto nearby stretched interfaces, and excess concentrations are expelled by desorption into the liquid where interfaces are compressed. Note that the colorbar range for $h = 0.01$ corresponds approximately one fifth that of

the colorbar for $h = 1$, as indicated by the brackets in Figure 5(a). Significantly more inhomogeneous concentration distributions are observed for $h = 1$ than for $h = 0.01$.

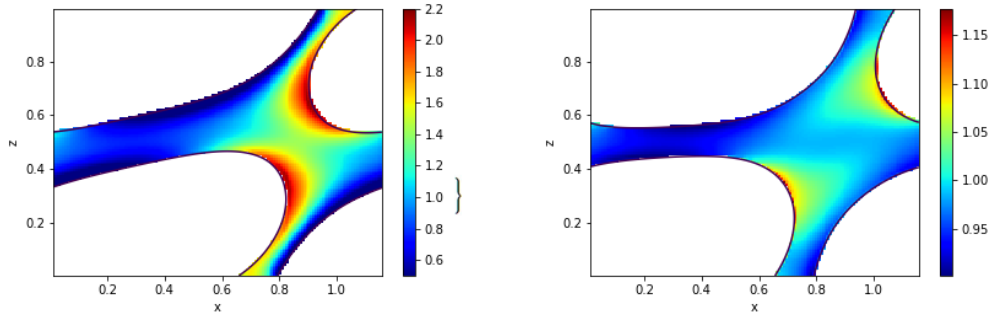

(a) $h = 1$ (b) $h = 0.01$

FIGURE 5 – Bulk concentration, F, in liquid bulk during T1 event. Top and bottom bubbles, in white, are moving to the right and left, respectively. (At equilibrium, $F_e = 1$.)

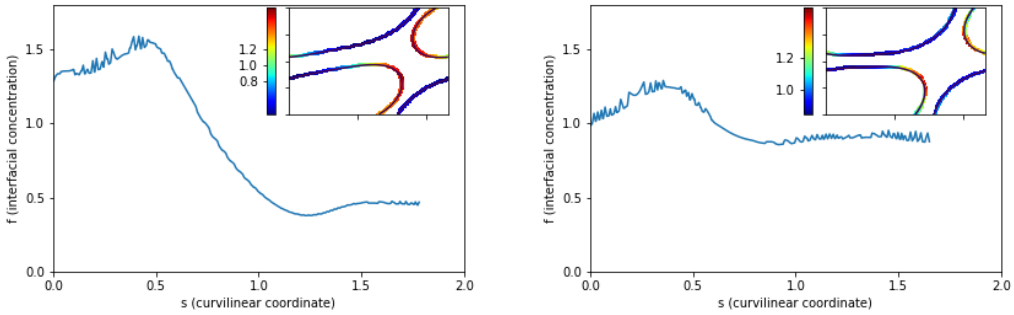

(a) $h = 1$ (b) $h = 0.01$

FIGURE 6 – Surface concentration, f, along the interface of bottom bubble. Inset : color maps for f. (At equilbrium, $f_e = 1$.)

The same dependence of surfactant distribution on adsorption depth is observed at interfaces. Surfactant concentration along the lower bubble surface is shown as a function of curvilinear coordinate, s, in Figures 6(a) and 6(b) for adsorption depths of $h = 1$ and $h = 0.01$. The curvilinear coordinate is oriented by the right hand rule with respect to the interior of the bubbles (Figure 4). We see stronger concentration gradients associated with the larger adsorption depth, and vice-versa (Figures 6(a) and 6(b)). Stronger concentration gradients also indicate stronger surface tension gradients, and therefore stronger Marangoni forces at the interface. At the interface scale, reduced adsorption depths tend to homogenize the surfactant distribution.

4.2 Energy balance

Power is injected to the fluid through work done by the walls as they maintain a steady shear. Total reaction forces at the walls can be computed as the sum of the capillary forces at contact lines, $\gamma_{wall} n_z sgn(n_x)$, and the viscous drag forces from the gas and liquid, $\int_{wall} \mu_{g,l} \left(\partial u_x / \partial z\right) dx$. From this, the total injected power required is obtained for steady wall shear as : $P_{inj} = F_{tot} U$. The total rate of viscous dissipation in the bulk is obtained by integration over the entire domain of the local viscous dis-

sipation rate of mechanical energy, which is derived as $\nabla \mathbf{u}$: $\left[\mu\left(\nabla \mathbf{u}+(\nabla \mathbf{u})^{T}\right)\right]$. From this, injected power can be compared to the viscous dissipation rate to infer how work is being done at the interfaces.

Figures 7(a) and 7(b) show the time evolution of the total injected power and integrated viscous dissipation rates for $h = 1$ and $h = 0.01$. This data corresponds to surfactant distributions shown previously, with $Pe = 100$. We have observed in all of our numerical experiments that both injected power and viscous dissipation decrease with decreased adsorption depth (figure 8(a)). The dotted lines show time averaged values of injected power, $\langle P_{inj}\rangle$, and integrated viscous dissipation rate, $\langle D_v\rangle$, in blue and yellow, respectively. Angled brackets denote a time average. Note that the injected power exceeds the total viscous dissipation rate. We see that the power delivered to the plates is not entirely dissipated by the bulk viscosity : $\langle P_{inj}\rangle > \langle D_v\rangle$. It was also found in the work of Titta et. al that part of the energy supplied by the moving plates must do work at the interfaces, and is associated with an effective surface dissipation, noted : $\langle D_s\rangle \equiv \langle P_{inj}\rangle - \langle D_v\rangle$[4].

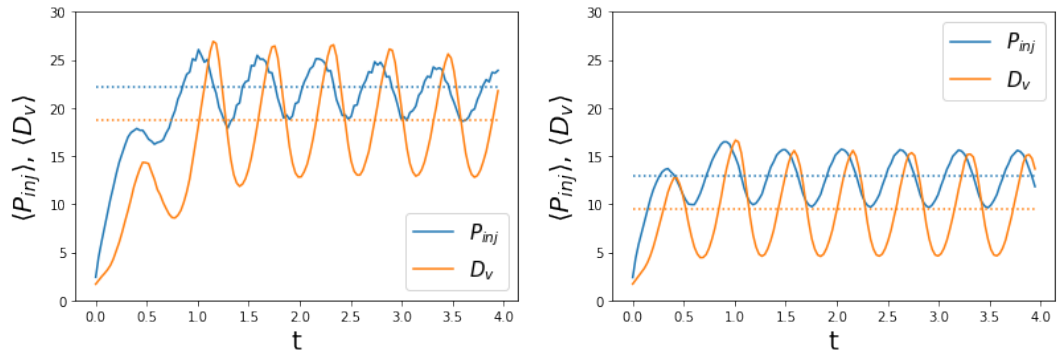

(a) $h = 1$ (b) $h = 0.01$

FIGURE 7 – Evolution of total injected power and viscous dissipation rates integrated over the fluid volume during steady wall-imposed shear. ($Pe = 100$, $Bi = 10$, $Ca = 0.1$)

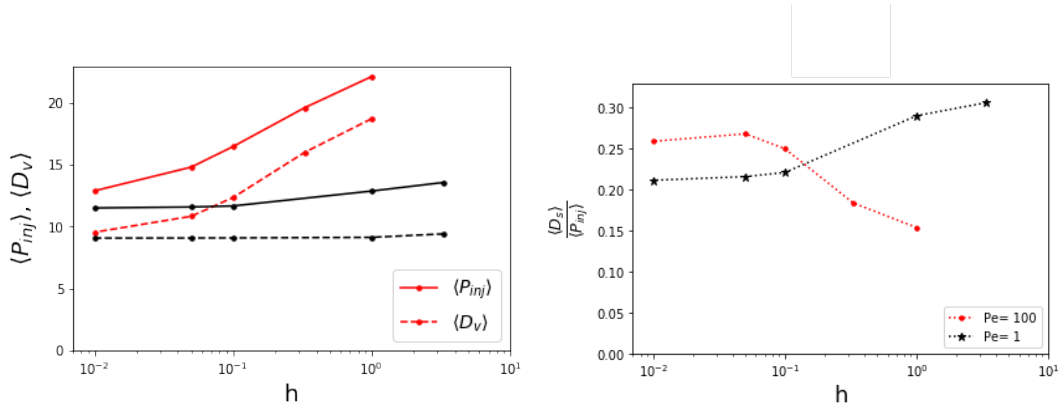

(a) $\langle P_{inj}\rangle$,$\langle D_v\rangle$ (b) $\langle D_s\rangle/\langle P_{inj}\rangle$

FIGURE 8 – Variation of injected power and dissipation rates with adsorption depth for diffusive and convective surfactant transport regimes. ($Bi = 10$, $Ca = 0.1$)

Figure 8(b) shows the contribution of effective surface dissipation to average injected power as a function of adsorption depth. The contribution of an effective surface dissipation is significant, ranging from about 16% to 30%. However, $\langle D_s\rangle/\langle P_{inj}\rangle$ is a decreasing function of h for $Pe = 100$ and an increasing

function of h for $Pe = 1$. There appears to be some coupled effect of adsorption depth and Péclet number on this effective surface dissipation.

5 Conclusions

We presented the level-set method for simulating T1 rearrangements of surfactant-laden 2D bubbles, and extended a parametric study initiated by Titta et al. to include the effects of the adsorption depth on the system dynamics. We found that, as the adsorption depth is decreased, surfactants tend to be more homogeneously distributed in the bulk and at the surface, and that the injected power required for maintaining a steady shear is reduced. We also found that there is a coupled effect of the Péclet number and the adsorption depth on the contribution of interfaces to energy dissipation in the fluid. This observed surface dissipation does not arise from an intrinsic surface viscosity. Rather, surface dissipation must be the result of a viscoelastic behavior of surfactant-laden interfaces arising from surfactant exchanges between the liquid bulk and its surface.

The global aim of this work is to shed light on shear rheology of larger bubble assemblies, and to eventually scale all the way to the foam level. First steps in this direction include :

— addition of intrinsic interfacial viscosity effects directly into the Navier-Stokes equations as source term. The viscous contribution to the interfacial forces can be rewritten in terms of an effective surface tension : $\gamma_{\text{eff}} = \gamma + (K^s + \mu^s)(\nabla_s \cdot \mathbf{u})$, where K^s and μ^s are respectively the dilational and shear interfacial viscosities.

— replacement of the solid plates (which are impermeable to surfactants) with some quasi-periodic boundary conditions to simulate the motion in an infinite bubble sheet

— extending the geometry to 3D bubbles

— simulation of drier systems - In current simulations, we consider foams with a 30% liquid volume fraction, which is roughly an order of magnitude greater than what is found in typical foams. At low liquid volume fraction, numerical diffusion of interfaces induce spurious events of bubble coalescence. We will attempt to implement multiple level-set functions to avoid these numerical (unphysical) coalescence events, and model drier bubble assemblies.

These objectives are part of the long term plans to develop more physically realistic simulations of T1 processes, and to obtain accurate rheological models for liquid foams.

Références

[1] I. Cantat, S. Cohen-Addad, F. Elias, F. Graner, R. Höhler, O. Pitois, F. Rouyer, and A. Saint-Jalmes. *Les mousses - Structure et dynamique*. Belin, 2010.

[2] A M Kraynik. Foam flows. *Annual Review of Fluid Mechanics*, 20(1) :325–357, 1988.

[3] Anne-Laure Fameau and Anniina Salonen. Effect of particles and aggregated structures on the foam stability and aging. *Comptes Rendus Physique*, 15(8) :748–760, October 2014.

[4] A. Titta, M. Le Merrer, F. Detcheverry, P. D. M. Spelt, and A.-L. Biance. Level-set simulations of a 2d topological rearrangement in a bubble assembly : effects of surfactant properties. *Journal of Fluid Mechanics*, 838 :222–247, 2018.

[5] E. K. Teigen, P. Song, J. Lowengrub, and A. Voigt. A diffuse-interface method for two-phase flows with soluble surfactants. *J. Comput. Phys.*, 230(2) :375–393, 2011.

[6] Andrea Titta. *Simulations level-set d'un amas de bulles cisaillées : écoulement et dynamique des tensioactifs*. PhD thesis, Université de Lyon, 2017.